

Selective Adsorption and Photocatalytic Clean-Up of Oil by TiO₂ Thin Film Decorated with p-V₃D₃ Modified Flowerlike Ag Nanoplates

Josiah Shondo, Salih Veziroglu, Tim Tjardts, Jacek Fiutowski, Stefan Schröder, Yogendra Kumar Mishra, Thomas Strunskus, Horst-Günther Rubahn, Franz Faupel, and Oral Cenk Aktas*


Various methods are developed and used to treat oil-contaminated water, including mechanical separation, chemical treatment, biological treatment, membrane filtration, and sorption. Oil clean-up via selective sorption of the oil by an engineered surface is the most accepted technique due to its high removal efficiency and low cost. Here, a multifunctional surface providing highly selective oil sorption and clean-up capability via the photocatalytic decomposition is proposed. This novel surface is named as the “three-in-one (3-in-1) surface” since it is composed of 1) a highly photocatalytic layer, 2) micro- and nanostructures, and 3) a low surface energy layer. First, the TiO₂ photocatalytic layer is prepared by magnetron sputtering. Then flowerlike Ag nanoplates are photocatalytically deposited on the sputtered TiO₂ layer. Afterward, a low surface energy layer, poly-1,3,5-trivinyl-1,3,5-trimethylcyclotrisiloxane (p-V₃D₃), is over-coated on Ag/TiO₂ surface by initiated chemical vapor deposition (iCVD) while retaining the topographical features of the surface (micro- and nanoscale surface structures). The p-V₃D₃/Ag/TiO₂ surface demonstrates a high selective adsorption to oil whereas simultaneously it shows extreme repellency to water. The p-V₃D₃/Ag/TiO₂ surface can also be photocatalytically cleaned up and this may find applications in various technology fields including water treatment, microfluidics, self-cleaning, and water harvesting.

1. Introduction

Increasing demand for petrochemical, mining, pharmaceutical, textile, metal processing, and food industries increases also the risk of water wasting by oil and oil-originated pollutants.^[1] Moreover, oil spill incidents during oil exploration and extraction, refining, and transportation form a high threat for water contamination.^[2,3] Various methods have been developed and used to treat oil-contaminated water including mechanical separation, chemical treatment, biological treatment, membrane filtration, and sorption.^[4–6] Among all these methods, oil clean-up via the sorption of the oil by an engineered surface is the most preferred method thanks to its ease of application, high removal efficiency, low cost, and as well as eco-friendly nature.^[7] An ideal sorbent material for oil clean-up should exhibit both high hydrophobicity and oleophilicity.^[8] Different types of materials possessing such a dual wettability nature (exhibiting both hydrophobicity and oleophilicity) has been proposed for the selective adsorption

J. Shondo, S. Veziroglu, T. Tjardts, S. Schröder, T. Strunskus, F. Faupel, O. C. Aktas
Chair for Multicomponent Materials
Institute of Materials Science
Faculty of Engineering
Kiel University
Kaiserstr. 2, 24143 Kiel, Germany
E-mail: oca@tf.uni-kiel.de

J. Fiutowski, Y. K. Mishra, H.-G. Rubahn
Mads Clausen Institute
NanoSYD
University of Southern Denmark
Alsion 2, Sønderborg 6400, Denmark
O. C. Aktas
Additive Manufacturing Excellence Centre – URTEMM
Kahramankazan, Ankara 06980, Turkey

 The ORCID identification number(s) for the author(s) of this article can be found under <https://doi.org/10.1002/admi.202102126>.

© 2022 The Authors. Advanced Materials Interfaces published by Wiley-VCH GmbH. This is an open access article under the terms of the Creative Commons Attribution License, which permits use, distribution and reproduction in any medium, provided the original work is properly cited.

DOI: 10.1002/admi.202102126

of the oil,^[9] on the other hand after adsorbing a certain amount of the oil, the surface of such materials are saturated and their oil removal capacity significantly goes down.^[10,11] Therefore, an ideal material surface should also exhibit recoverability of the adsorbed oil in addition to hydrophobicity and oleophilicity for the efficient oil clean-up. In recent years, using materials that show preferential wetting and nonwetting characteristics, have gained tremendous interest in developing oil clean-up technologies.^[12]

In this current work, we propose a novel surface that exhibits highly selective oil adsorption and clean-up capability via the photocatalytic decomposition of the adsorbed oil. We developed so-called three-in-one (3-in-1) surface composed of 1) a highly photocatalytic layer, 2) micro- and nanostructures, and 3) a low surface energy layer. The photocatalytic layer was prepared by the magnetron sputtering of TiO₂ and then Ag structures were photocatalytically deposited onto this active layer to achieve stable micro- and nanoscale topographic features. Afterward, a low surface energy layer (poly-1,3,5-trivinyl-1,3,5-trimethylcyclotrisiloxane, p-V₃D₃), was deposited onto the Ag/TiO₂ surface by the initiated chemical vapor deposition (iCVD). The iCVD technique allows a well-controlled film thickness (down to 5–10 nm) promoting the retention of the surface topography (morphology of flowerlike Ag nanoplates and columnar TiO₂ structures), which is necessary to achieve superhydrophobic state. Photocatalytic p-V₃D₃/Ag/TiO₂ surface demonstrates a high adsorption selectivity toward oil whereas simultaneously it shows an extreme repellency to water. Adsorbed oil can be decomposed photocatalytically under UV light and then p-V₃D₃/Ag/TiO₂ surface can be reused for oil–water separation. Due to its siloxane backbone, the p-V₃D₃ layer seems to exhibit high stability to UV irradiation and atomic oxygen exposure. The proposed 3-in-1 surface concept may

find applications in oil–water separation, microfluidics,^[13] self-cleaning, and water harvesting^[12] technologies.

2. Results and Discussion

The preparation of p-V₃D₃/Ag/TiO₂ and PTFE/Ag/TiO₂ (used as a control substrate for comparison) surfaces follows three steps approach: i) preparation of TiO₂ thin film, ii) photocatalytic deposition of flowerlike Ag nanoplates, and iii) deposition of polymer layers via iCVD as schematically shown in **Figure 1**.

To investigate the surface morphology of the photocatalytically deposited flowerlike Ag nanoplates, helium ion microscope (HIM) was utilized as presented in **Figure 2**. Previously, we showed that Ag⁺ ions were reduced to stable and globular Ag nanostructures on TiO₂ thin films under UV illumination (4.5 mW cm² UV lamp operating at $\lambda = 365$ nm).^[14] We demonstrated that the formation of such Ag nanostructures was mainly governed by photoexcited charge carriers generated in TiO₂ during photocatalytic reactions. However, in this work, we used trisodium citrate (Na₃C₆H₅O₇) as the reducing agent and we observed a quite different morphology in comparison to those which we reported previously.^[14] Therefore, the growth mechanism of Ag nanoplates should be different. We assume that the first photoexcited charge carriers generated by TiO₂ induced the photooxidation of the citrate (C₆H₅O₇) and this leads to the decarboxylation to organic radicals. Then, these radicals seem to be chemisorbed onto Ag⁺ ions via the electron transfer and finally, Ag⁺ ions are reduced to immobilized stable metallic Ag structures on the TiO₂ surface.^[15] It seems that the arrangement of interconnected Ag nanoplates results in the formation of flowerlike Ag structures as shown in **Figure 2a,b**. The elemental mapping of silver (Ag), titanium (Ti), and oxygen (O) by scanning electron microscopy–energy

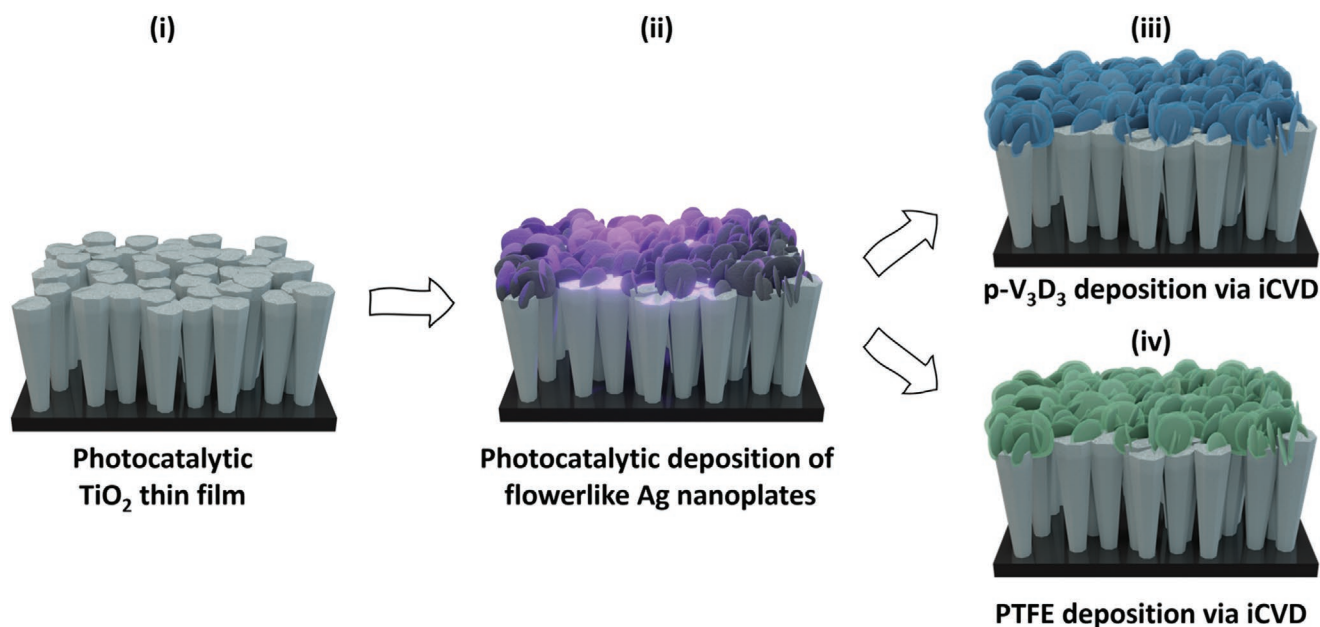


Figure 1. i) Sputter-deposited TiO₂ thin film, ii) photocatalytic deposition of flowerlike Ag nanoplates on TiO₂ thin film, iii) p-V₃D₃ deposition on Ag/TiO₂ via iCVD, and iv) PTFE (as control substrate) deposition on Ag/TiO₂ via iCVD.

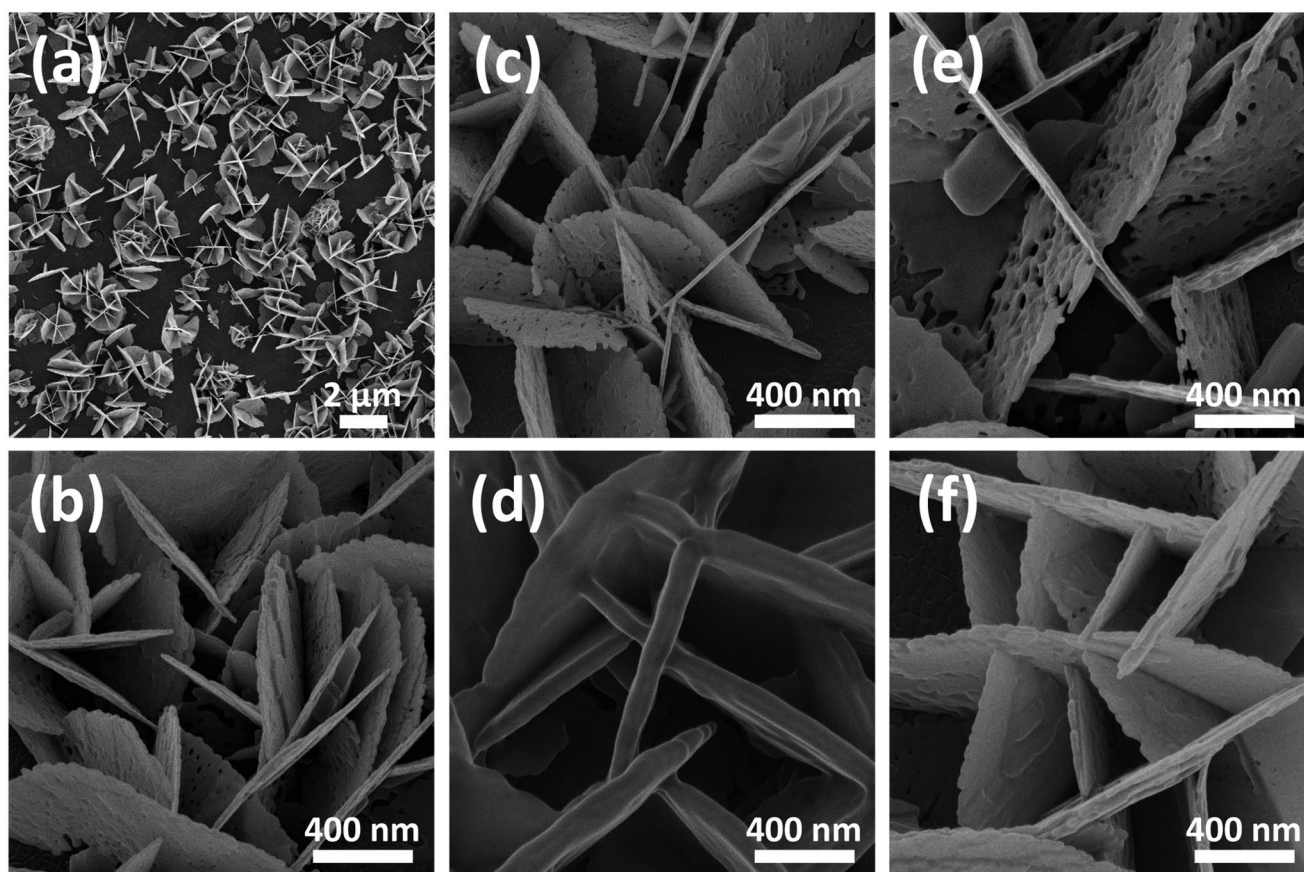


Figure 2. HIM images of photocatalytically deposited flowerlike Ag nanoplates on TiO_2 a) at low and b) at high magnification. HIM images of photocatalytically deposited flowerlike Ag on TiO_2 after over-coating with a c) 25 nm $\text{p-V}_3\text{D}_3$ layer and d) 100 nm $\text{p-V}_3\text{D}_3$ layer, e) 25 nm PTFE layer, and f) 100 nm PTFE layer.

dispersive spectroscopy (SEM-EDS) demonstrates the presence of TiO_2 decorated with flowerlike Ag nanoplates shown in Figure S1 of the Supporting Information (the additional silicon (Si) mapping results from the Si-wafer substrate).

The X-ray diffraction (XRD) analysis revealed the preferential orientation of flowerlike Ag nanoplates in (111) direction as shown in Figure S2 of the Supporting Information. Various studies proposed different mechanisms for the growth of Ag structures in nanoplate form. Especially in the case of photochemical synthesis routes, it is believed that dipole plasmon excitation may induce an ultrafast charge separation on Ag nanostructures surface and this triggers the face-selective reduction of Ag^+ ions and anisotropic crystal growth.^[16] Moreover, during photocatalytic reactions, H_2O_2 may counterattack the reduction of Ag^+ by $\text{C}_6\text{H}_5\text{O}_7^-$. This may lead to the formation of Ag seeds with (111) twin planes and stacking faults. It is known that such seeds are more stable against oxidative etching, and they grow at the expense of less stable nanoparticles with smaller sizes and/or other shapes (they dissolve in O_2 rich medium and serve as the Ag^+ source for the nanoplate growth).^[17]

Figure 2c,d presents HIM images of 25 and 100 nm thick $\text{p-V}_3\text{D}_3$ over-coated Ag/TiO_2 , respectively. Similarly, Figure 2e,f shows PTFE over-coated Ag/TiO_2 (with the thickness of 25 and 100 nm, respectively). HIM images showed no significant

change in the morphology of Ag structures before and after the deposition of the polymer layers. This confirms that iCVD leads to a highly conformal coating. Since it was not possible to distinguish deposited polymer layers on Ag/TiO_2 surface via HIM analysis, the presence of $\text{p-V}_3\text{D}_3$ and PTFE layers were revealed by X-ray photoelectron spectroscopy (XPS) analysis. Wide-scan XPS spectrum survey shows C 1s, F 1s, O 1s, Ag 3d, and Ti 2p peaks as presented in Figure 3a,b for $\text{p-V}_3\text{D}_3$ and PTFE over-coated Ag/TiO_2 , respectively. In the XPS spectrum of $\text{p-V}_3\text{D}_3$ over-coated samples, as expected we observed the Si 2p peak, which is a clear indication of the silicon backbone of $\text{p-V}_3\text{D}_3$ (a high-resolution spectrum is given in Figure 3c).

In comparison to XPS spectra of 25 nm thick polymer layers over-coated Ag/TiO_2 surfaces, we observed a decrease in intensities of Ag 3d and Ti 2p peaks for 100 nm thick polymer layers over-coated Ag/TiO_2 surfaces, which is a clear consequence of the increase in over-coated polymer thickness.^[18] In addition, we observed a slight difference between morphologies of 100 nm thick $\text{p-V}_3\text{D}_3$ and PTFE layers. While the 100 nm thick $\text{p-V}_3\text{D}_3$ layer exhibited a high conformality, we observed some protrusion type inhomogeneities at the 100 nm thick PTFE layer, which may be due to the lack of the good adhesion between PTFE films and Ag nanoplates (Figure 2f). The $\text{p-V}_3\text{D}_3$ layer seems to have better adhesion affinity to the Ag/TiO_2 surface which may be due to the Si–O backbone of $\text{p-V}_3\text{D}_3$.^[19,20]

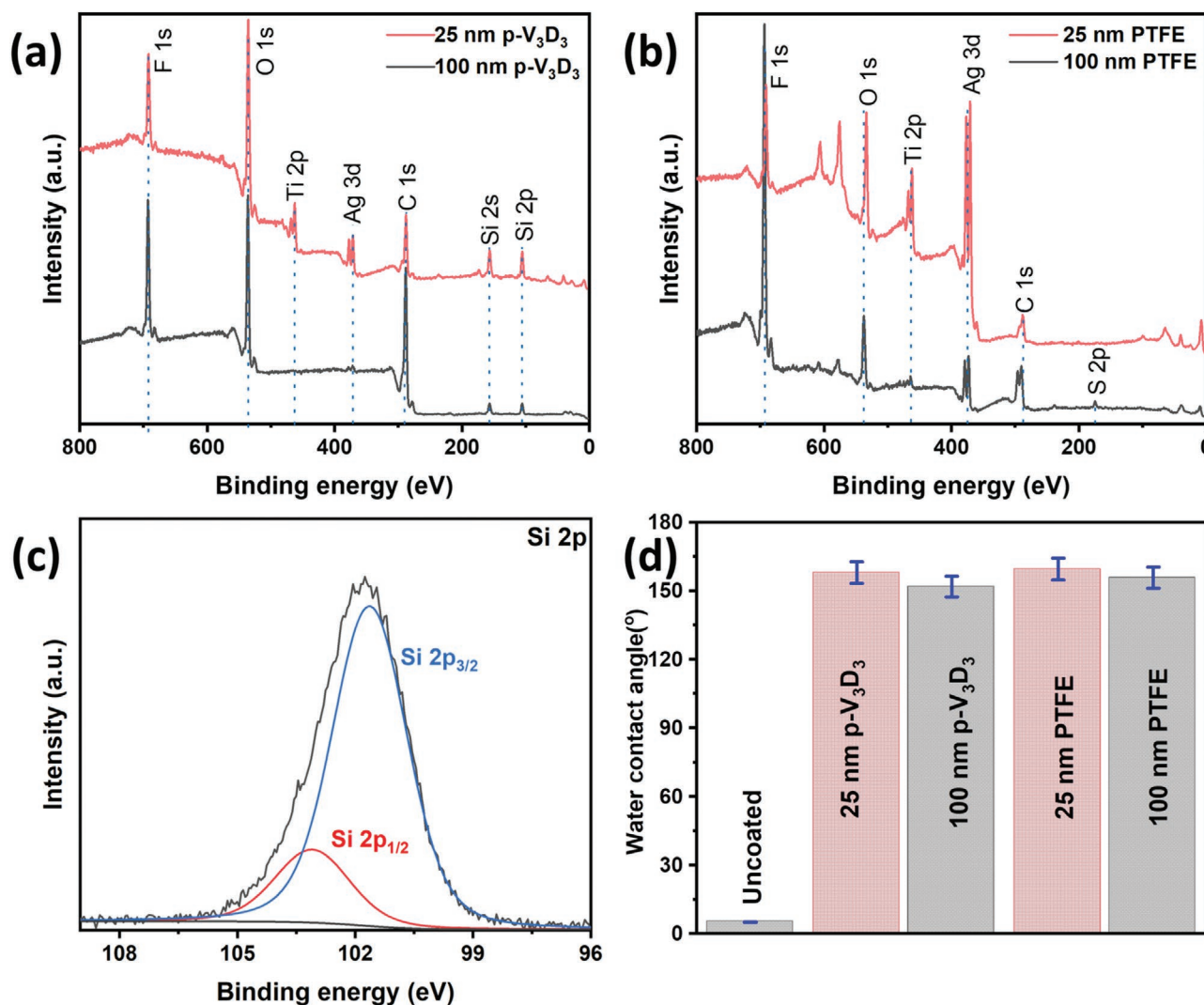


Figure 3. a) XPS spectra of 25 nm and 100 nm thick p-V₃D₃ over-coated Ag/TiO₂ surfaces, b) XPS spectra of 25 and 100 nm thick PTFE over-coated Ag/TiO₂ surfaces, c) high-resolution Si 2p XPS spectrum of 25 nm thick p-V₃D₃ over-coated Ag/TiO₂ surface, and d) water contact angle (WCA) analysis of p-V₃D₃ and PTFE coated samples at respective thicknesses (static, advancing, receding, and sliding WCAs are given in Table S1, Supporting Information).

Using a semiautomated goniometer, we investigated the effects of Ag/TiO₂ surface features and polymer layers (p-V₃D₃ and PTFE) on the wettability. As shown in various studies including ours, TiO₂ exhibits a hydrophilic nature and under the UV light a superhydrophilic state can be achieved.^[21–23] In Figure 3d one can see that the TiO₂ layer showed a water contact angle (WCA) around 5° after photocatalytic deposition of the Ag structures. Indeed, this is in agreement with Wenzel's rule which states that an intrinsically hydrophilic material will become more hydrophilic by increasing the surface roughness and/or introducing hierarchical roughness.^[24–27] To further confirm the surface roughness, which plays an important role in enhancing the wettability properties of flowerlike Ag nanoplates on TiO₂, the surface topography of the prepared samples was analyzed by atomic force microscopy (AFM) as shown in Figure S3 of the Supporting Information. The average surface roughness (Ra) and root mean square roughness (rms) were

measured as 704.4 (± 24.6) nm and 744.8 (± 26.1) nm for Ag/TiO₂ and 18.9 (± 1.1) nm and 23.8 (± 1.3) nm for bare TiO₂, respectively; which clearly indicates a significant change in surface roughness after photocatalytic deposition of flower like Ag nanoplates.^[28] After the deposition of p-V₃D₃ and PTFE layers, we observed a transition from the superhydrophilic state to a superhydrophobic state. Although all iCVD modified samples exhibited a superhydrophobic state (WCA > 150°) regardless of the type and thickness of the deposited layers, the highest WCA of 163° was observed in the case of the 25 nm p-V₃D₃ over-coated Ag/TiO₂ surfaces. Furthermore, we observed that iCVD modified surfaces were not only superhydrophobic but also, showed superoleophilic properties with an oil contact angle (OCA) below 6° (Figure S4, Supporting Information).

To further reveal the superhydrophobic and superoleophilic behavior of the p-V₃D₃/ Ag/TiO₂ sample, we recorded the interaction of water and oil droplets with the surface with

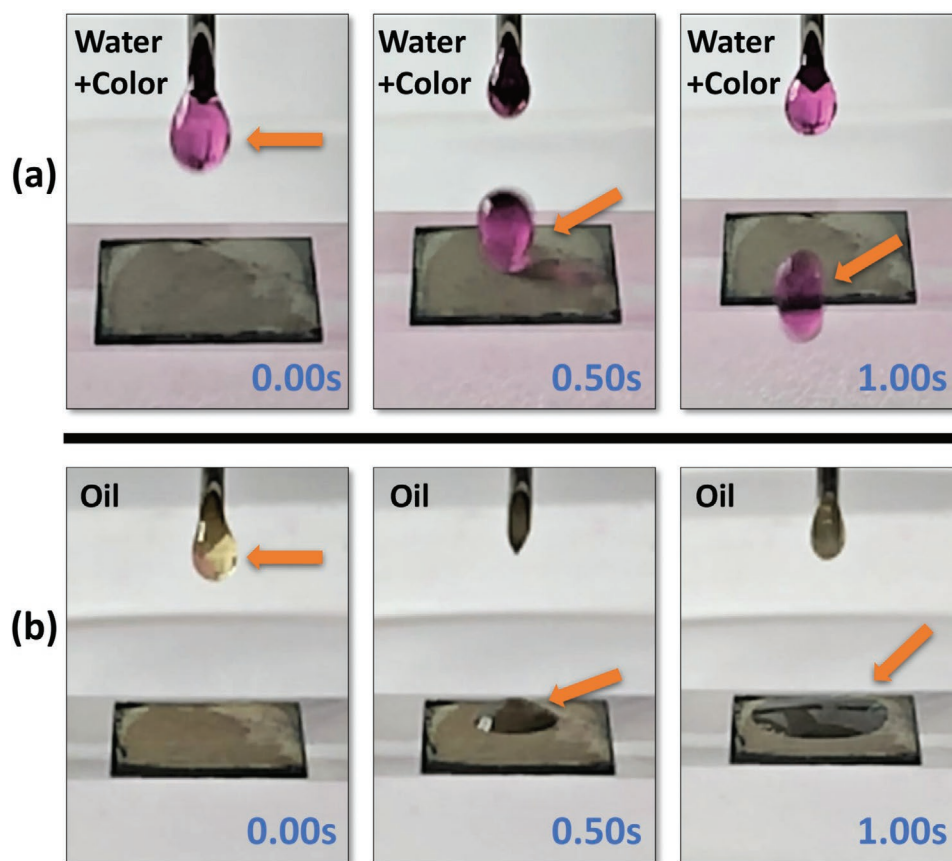


Figure 4. a) Bouncing of the water droplet (colored with pinkish dye) on $p\text{-V}_3\text{D}_3/\text{Ag}/\text{TiO}_2$ surface and b) spreading of the oil droplet on $p\text{-V}_3\text{D}_3/\text{Ag}/\text{TiO}_2$ surface (orange arrows represent the position of the droplets).

a high-speed camera (Videos S1 and S2, Supporting Information). By tilting the base plane of the semiautomated contact angle goniometer with help of a precise micromanipulator, we measured a sliding angle of $6^\circ\text{--}8^\circ$ which indicates high water repellence. For instance, as soon as the water droplet impacted the $p\text{-V}_3\text{D}_3/\text{Ag}/\text{TiO}_2$ surface it bounced and completely left the surface as shown in **Figure 4a**. We did not observe any residual from water droplets (colored with E127 Eritrosina dye, E127 eritrosina granular B20g supplies by Fast colors LLP). When the same volume of an oil droplet contacted with $p\text{-V}_3\text{D}_3/\text{Ag}/\text{TiO}_2$ surface, the droplet spread out rather than bouncing on the surface (as observed in the case of the water droplet) as shown in **Figure 4b**.

In addition, to demonstrate the oil adsorption properties of $p\text{-V}_3\text{D}_3/\text{Ag}/\text{TiO}_2$ surface first, we prepared an oil contaminated water model by drop-casting a limited amount of motor-oil into water. Afterward, the $p\text{-V}_3\text{D}_3/\text{Ag}/\text{TiO}_2$ sample was immersed into the prepared oil–water mixture as shown in **Figure 5** and Video S8 (Supporting Information). By moving the $\text{V}_3\text{D}_3/\text{Ag}/\text{TiO}_2$ sample back-and-forth in oil–water mixture, the oil droplets were captured. The selective capturing of oil droplets clearly indicates an oleophilic state of the surface in addition to its superhydrophobicity.

The dual nature, superhydrophobicity and superoleophilicity, of $p\text{-V}_3\text{D}_3/\text{Ag}/\text{TiO}_2$ surface forms a good basis for an effective oil–water separation. On the other hand, the cumulative oil

adsorbate by the time may hinder the oil–water separation performance in the long term. The adsorbed oil needs to be eliminated from the surface to achieve a sustainable oil–water separation. To investigate the photocatalytic clean-up capability of the prepared $p\text{-V}_3\text{D}_3/\text{Ag}/\text{TiO}_2$ surface a motor-oil droplet with a volume of $5\ \mu\text{L}$ was spread out on $p\text{-V}_3\text{D}_3/\text{Ag}/\text{TiO}_2$ surface to induce an artificial contamination. Just after spreading out of the oil droplet on $p\text{-V}_3\text{D}_3/\text{Ag}/\text{TiO}_2$ surface, the corresponding WCA dropped to 90° . This is a clear indication of surface contamination since the same surface exhibited a superhydrophobic state (with a WCA of 162.8°) before spreading of the oil droplet. Then $p\text{-V}_3\text{D}_3/\text{Ag}/\text{TiO}_2$ surface was exposed to UV light (with the intensity of $5.85\ \text{mW cm}^{-2}$ operating at $\lambda = 365\ \text{nm}$) and the change in WCA was monitored at defined time frames. By the time a gradual recovery of the hydrophobicity was observed as shown in **Figure 6a**. A similar recovery was also observed for the oil-contaminated PTFE/ Ag/TiO_2 surface (used as a comparison) as shown in **Figure 6b**.

Previously, we showed that the photocatalytic activity of TiO_2 thin films can be enhanced by the incorporation of Ag nanostructures on the TiO_2 surface.^[14] Basically, this occurs by inhibiting the recombination of photoexcited charge carriers (electron–hole (e^-/h^+)) due to the electron affinity of Ag nanostructures.^[29] Therefore, in case of TiO_2 layer decorated with flowerlike Ag nanoplates photoexcited charges might be easily transferred from the semiconductor (e.g. TiO_2) to the matching

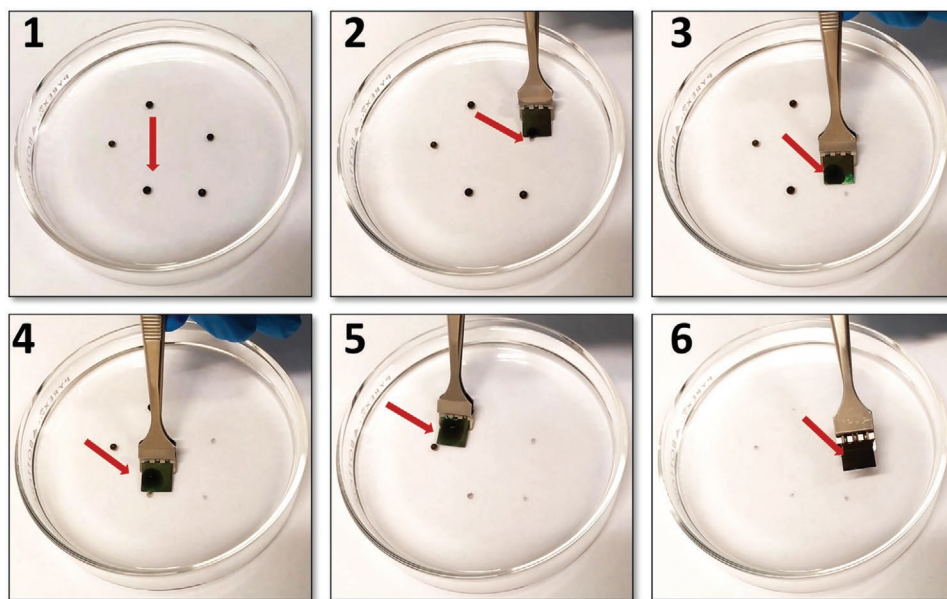


Figure 5. Selective capturing of oil droplets from motor oil–water mixture by $p\text{-V}_3\text{D}_3/\text{Ag}/\text{TiO}_2$ surface (1) motor oil droplets in water and (2–6) selective adsorption of motor oil droplets on $p\text{-V}_3\text{D}_3/\text{Ag}/\text{TiO}_2$ from water.

energy level of metallic structures (e.g. Ag nanoplates).^[30,31] On the other hand, in case of $p\text{-V}_3\text{D}_3/\text{Ag}/\text{TiO}_2$ and $\text{PTFE}/\text{Ag}/\text{TiO}_2$ the top-polymer layer acts as the dielectric layer (especially $p\text{-V}_3\text{D}_3$ is known to have a large bandgap of 8.25 eV),^[32] which makes the charge transfer and separation mechanism more complicated. Kamegawa et al. showed that the composite layer composed of TiO_2 and PTFE exhibited a strong photocatalytic activity and authors claimed that PTFE promotes the charge separation.^[33] Similarly, Ibhaden et al. showed that SiO_2 particles deposited onto TiO_2 induced an efficient separation of electron–hole pairs and this increased the photocatalytic activity of TiO_2 .^[34] Moreover, Mahesh Reddy et al. reported a similar mechanism for the strong photocatalytic activity of polyurethane-modified TiO_2 .^[35] By comparing our result with these findings, we resolve that the ultrathin nature of PTFE and $p\text{-V}_3\text{D}_3$ polymer layers seem to allow the electron transfer to the surface from Ag/TiO_2 layer beneath. This allows the photodegradation of adsorbed oil (e.g. hexadecane) on the surface and renders the superhydrophobic state.^[36] In addition to its effect on the charge-separation, the top-layer covering Ag/TiO_2 seems to promote the photocatalytic performance by increasing the overall optical absorption as shown by measuring their UV–vis spectra (Figure S5a, Supporting Information). The optical spectrum of bare TiO_2 shows a clear cut-off wavelength at 352 nm corresponding to a bandgap of 3.52 eV (Figure S5b, Supporting Information), which is in agreement with reported bandgap values for sputter deposited TiO_2 (e.g. anatase) thin films.^[37–39] On the other hand, we observed a significant shift of the optical spectrum to higher wavelengths (with a new value of the cut-off wavelength film remains high) after over coating Ag/TiO_2 surface with polymer top-layer. It is difficult to reveal the bandgap of $p\text{-V}_3\text{D}_3/\text{Ag}/\text{TiO}_2$ by simply Tauc plot since flower-like Ag nanoplates are composed of hierarchical plasmonic. In addition, the presence of a nonhomogenous optical medium, $p\text{-V}_3\text{D}_3/\text{Ag}/\text{TiO}_2$ (cross-sectional look at the presence of Ag

structures) and $p\text{-V}_3\text{D}_3/\text{TiO}_2$ (cross-sectional look at absence of Ag structures) makes it a complicated optical system. Nevertheless $p\text{-V}_3\text{D}_3/\text{Ag}/\text{TiO}_2$ exhibited much higher optical absorption in comparison to bare TiO_2 , which may clearly contribute to the overall photocatalytic performance.

For further evaluation of the photocatalytic clean-up performance of $p\text{-V}_3\text{D}_3/\text{Ag}/\text{TiO}_2$, the 100 nm thick $p\text{-V}_3\text{D}_3$ coated sample surface was contaminated by oleic acid (volume: 10 μL) and then exposed to UV light for 3 h while visually monitoring the surface as shown schematically in Figure 6c. After exposing the sample to UV light for 1 h, we could notice a gradual decrease in the volume of oleic acid on the surface and after 3 h barely any residual from oleic acid could be seen on the surface (Figure 6d). A quick check with the goniometer showed that the surface kept its superhydrophobic state with water WCA > 154°. On the other hand, the TiO_2 thin film surface was also contaminated with oleic acid and exposed to UV light for 10 h. XPS investigation showed a gradual decrease in peak intensity and concentration % of C 1s while those increase in case of both Ti 2p and O 1s (Figure S6 and Table S2, Supporting Information).^[40] Here, high stability of the $p\text{-V}_3\text{D}_3$ coating might arise due to the presence of the Si–O bond (which can also promote a strong adhesion of the polymer layer to the Ag/TiO_2 surface).^[19] This clearly shows that a $p\text{-V}_3\text{D}_3$ layer is more suitable than the conventional PTFE coating for oil–water separation and photocatalytic clean-up application. Moreover, such a $p\text{-V}_3\text{D}_3$ layer (100 nm) has a high potential to replace PTFE also due to its eco-friendly nature.

Ag/TiO_2 shows high photocatalytic activity for clean-up of the oil contamination. Conversely, one should think that photocatalytic reactions may lead to the degradation of the polymer layers used as the top-coat. For instance, as shown in Figure 6a we observed a decrease in WCA on the 25 nm thick $p\text{-V}_3\text{D}_3$ over-coated Ag/TiO_2 after 5 h, which indicates a possible photocatalytic decomposition of the $p\text{-V}_3\text{D}_3$ layer. The XPS

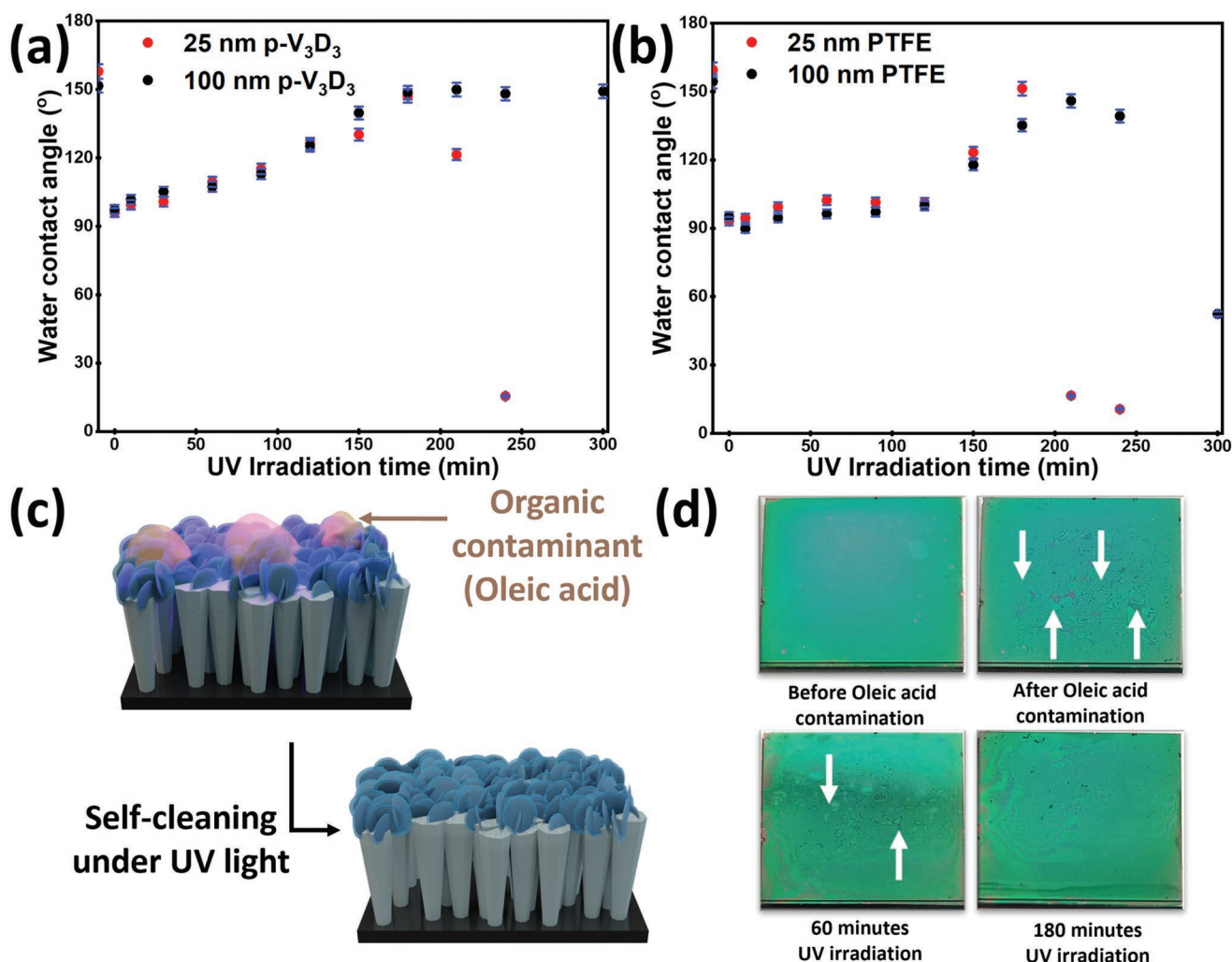


Figure 6. Change in water contact angle (WCA) by the contamination of the sample surface by hexadecane oil and the photocatalytic clean-up under UV light irradiation for a) p-V₃D₃ and b) PTFE-coated samples. c) Schematic of the photodegradation process and d) photocatalytic clean-up of oleic acid residue on the sample surface under UV light irradiation.

analysis revealed that p-V₃D₃ layer alone without the active Ag/TiO₂ layer does not show any self-decomposition under UV irradiation as shown in Figure S7 of the Supporting Information.

In comparison, the 25 nm p-V₃D₃ layer showed a much higher UV stability than the 25 nm PTFE layer as shown in Figure 6b. As expected, the stability of deposited polymer layers against exposure to UV light and photocatalytic self-degradation reactions was improved with the increasing thickness of the deposited polymer top-layer. Figure 6a shows that the 100 nm thick layers showed high WCAs after 300 min of UV irradiation, which indicates high stability of the layers against UV light and as well as photocatalytic reactions (self-degradation). So, one needs to think about a compromise between enhancing the stability of the deposited layers and retention of surface topography (which is essential for attaining high WCAs) while choosing a proper thickness.

The robustness of the p-V₃D₃ coated surface (100 nm) was further tested against the chemical shielding effect^[41] in both acidic (3 M H₂SO₄ and 3 M HCl, Sigma-Aldrich, Germany) and

alkaline (3 M NaOH and 3 M KOH, Sigma-Aldrich, Germany) medium (Videos S3–S6, Supporting Information). There were no visible reactions after 2 min (commonly waiting for 1 min) of immersion in both acids and bases. Most interestingly, the WCA of the surface showed no significant changes (Table S3, Supporting Information) after chemical stability tests. We further tested robustness of the surface under a pressurized water jet. After a continuous flow of the pressurized water on the surface for an hour, the surface still retained its superhydrophobicity (Figure S8 and Video S7, Supporting Information).

The change in surface chemistry of p-V₃D₃/Ag/TiO₂ after photocatalytic reaction induced by the exposure to UV light was further investigated with XPS (Figures S9 and S10, Supporting Information). The XPS analysis showed a slight decrease in surface atomic concentrations of C 1s and F 1s after exposure to UV light (Table S4, Supporting Information). The oxygen (O) to carbon (C) ratio was observed to steadily increase with UV irradiation due to oxygen-containing species on the surface (at a binding energy of 532.8 eV, which is assigned to typical oxygen

functional groups as carbonyl and siloxane).^[42] This shows that both UV irradiation and as well as photocatalytic reactions affect the overall stability of polymer top-layer, thus the hydrophobicity. By comparing the change in the intensity of F1s peak after exposure to UV light (Figure S11, Supporting Information), it is obvious that the 25 nm PTFE layer exhibited much lower stability than the 25 nm p-V₃D₃ layer. Siloxane backbone seems to endorse the stability of p-V₃D₃, and this promotes the reusability of p-V₃D₃/Ag/TiO₂ for oil–water separation after the photocatalytic clean-up. The 3-in-1 surface, p-V₃D₃/Ag/TiO₂, may be used in various oil–water separation and self-cleaning applications.

3. Conclusion

In summary, we prepared a stable superhydrophobic and photocatalytically active surface by the 3-in-1 approach which combines 1) photocatalytic thin film, 2) micro- and nanostructuring via photocatalytic deposition, and 3) low surface energy coating via iCVD. Our results show that not only p-V₃D₃ coating, but also the unique surface topography composed of flowerlike Ag nanoplates and columnar TiO₂ structures promoted the superhydrophobicity of the surface. iCVD led to a highly conformal p-V₃D₃ coating retaining the surface topography on TiO₂, which is crucial to achieve an extreme non-wetting regime. Additionally, due to its siloxane backbone, the p-V₃D₃ layer exhibited high stability against the UV irradiation and atomic oxygen exposure (photodegradation). The superhydrophobic (WCA > 160°) and photocatalytically active p-V₃D₃/Ag/TiO₂ surface shows high selectivity to oil adsorption, which may lead to several functional applications in oil–water separation, microfluidics, self-cleaning, and water harvesting technologies.

4. Experimental Section

Preparation of TiO₂ Thin Film: TiO₂ thin film with a thickness of 500 nm was deposited by DC magnetron sputtering from 2 in. titanium (Ti) target in a custom-built vacuum deposition chamber.^[43,44] Silicon wafer pieces (10 mm × 10 mm) were used as substrates. Before the deposition of TiO₂ thin film, a base pressure of 10^{−5} Pa was achieved by using a fused rotary (Agilent Technologies, SH-110) in combination with a turbo molecular pump (Pfeiffer Vacuum, HiPace 400). Initially, the Ti target (Goodfellow, 99.99% with a 50 mm diameter) was cleaned in a pure Ar plasma for 10 min followed by a conditioning phase of 5 min with both argon (Ar) and oxygen (O₂) flow. The deposition was conducted (for 90 min) at a magnetron output power of 90 W while keeping the gas flow ratio of Ar (process gas):O₂ (reactive gas) at 250:5 by using two separate mass flow controllers (MKS Multi-Gas-Controller 647C). To achieve a homogenous TiO₂ film, the sample holder was rotated during the deposition. Following the deposition process, the samples were heat-treated for 1 h at 650 °C in an oven (Nabertherm, LE 4/11/R6) and subsequently air quenched to induce a nanocracks network (leading to high surface area) in the TiO₂ columnar structures, as described before.^[45]

Photocatalytic Deposition of Flowerlike Ag Nanoplates on TiO₂ Thin Films: Aqueous solutions of silver nitrate (AgNO₃, Sigma-Aldrich, Germany) and trisodium citrate (Na₃C₆H₅O₇, Sigma-Aldrich, Germany) were prepared separately at concentrations of 0.003 m and 0.3 m, respectively. Then the freshly prepared TiO₂ thin film samples were dipped into a quartz cuvette filled with 6.5 mL of AgNO₃ solution, 200 μL Na₃C₆H₅O₇ solution, and 50 μL of Triton-X100 (Carl-Roth,

Germany). Additionally, tetramethylammonium hydroxide and nitric acid (HNO₃ Sigma-Aldrich, Germany) were used to adjust the pH (Tester kit pH 5, supplied by Carl Roth GmbH+Co.KG) value of the solution to 2.2. Afterward, samples were exposed to low-intensity (4.5 mW cm^{−2}) UV irradiation (using UV LED StellarNet EPP2000C-SR-50 with SL5-DH light source, operating at a wavelength of 365 nm) through the quartz cuvette for 10 min. Subsequently, the samples were rinsed with deionized water to remove excess solution left on the surface and air-dried at room temperature.

Deposition of Polymer Layer by iCVD: p-V₃D₃ layer was deposited on prepared Ag/TiO₂ samples in a custom-built iCVD reactor system operated in a constant flow mode, as described before.^[27,46,47] First the reactor was evacuated for at least 3 h before introducing the monomer (1,3,5-trivinyl-1,3,5-trimethylcyclotrisiloxane, V₃D₃-ABCR, Germany) and the initiator perfluorobutanesulfonyl fluoride (PFBSF, 95% Fluorochem, UK). The reactor pressure was set to 50 Pa and controlled by a downstream butterfly valve (VAT Series 615), coupled to a capacitance manometer (MKS Baratron), that is connected to the reactor. V₃D₃ monomer was heated in a custom-made jar to 60 °C and delivered through a precise metering valve (Swagelok, Germany) to the reactor. Then the flow of the initiator and the monomer were calibrated. Flow rates were set to 0.2 and 0.1 sccm for V₃D₃ and PFBSF, respectively. By keeping calibrated flow constant Nichrome (Ni/Cr: 80/20, Goodfellow GmbH) filaments were resistively heated at a filament power of 38.3 W and the sample stage was kept at 30 °C using water cycling through a thermostat (Huber CC-K6). For 25 nm thickness and 100 nm thickness, the deposition time was adjusted to 7 and 28 min, respectively.

A similar procedure was applied to the deposition of the PTFE layer on Ag/TiO₂ (as control substrate). Here, the PFBSF monomer and the initiator hexafluoropropylene oxide (97%, Fluorochem, UK) were mixed at a ratio of 0.2. The filament power of 35.5 W was applied during the deposition to the Nichrome filament array. During the deposition, the sample stage was cooled to 20 °C by the water circulating thermostat. The process pressure inside the reactor was set to 50 Pa controlled by the downstream butterfly valve. To achieve 25 nm thickness and 100 nm thickness, the deposition time was adjusted to 7.5 and 29.5 min, respectively.

Characterization: The surface morphology and the structure of the prepared samples were characterized by helium ion microscope (HIM, Orion NanoFab-Carl Zeiss) and scanning electron microscope (SEM, Supra55VP-Carl Zeiss) integrated energy-dispersive (EDS, Ultim Max 65-Oxford) detector. The surface roughness of the bare TiO₂ and TiO₂ decorated with flowerlike Ag nanoplates was determined using an AFM operating at oscillating cantilever (AC) mode (WITec Alpha 300 RA). The Ra and rms were quantified using an open access software Gwyddion 2.59. The surface chemistry of the samples was analyzed by XPS (Omicron Nano-Technology GmbH, Al anode, 240 W). CasaXPS software (2.3.13PR1.0) was used to perform quantitative analyses and detailed peak investigation. All binding energies (BE) were calibrated with reference to the Ag 3d line at 368.3 eV of silver on the sample surface. WCA measurements were performed using a semiautomated contact angle goniometer (OCA 30, Dataphysics). For static WCA measurements water droplets with a volume of 10 μL were used, and advancing/receding angles were recorded by the addition and subtraction of water gradually as explained by Tadmor.^[48] The XRD measurement of prepared samples was carried out using a 9 kW rotating Cu anode X-ray source (λ ≈ 1.54 Å) in a Grazing incidence XRD setup with omega (ω) of 0.7 at a scanning rate of 2° min^{−1} with high-quality semiconductor detector that supports 0D, 1D or 2D X-ray diffraction measurement (Rigaku SmartLab), operating at the voltage of 45 kV and a current of 200 mA.

Supporting Information

Supporting Information is available from the Wiley Online Library or from the author.

Acknowledgements

J.S. and S.V. contributed equally to this work. J.S. wishes to thank DAAD (Deutscher Akademischer Austauschdienst) and PTDF (Petroleum Technology Development Fund) for providing funding for his doctoral studies. The authors thank NanoBMT Co. Ltd. for wetting analysis of prepared surfaces.

Open access funding enabled and organized by Projekt DEAL.

Conflict of Interest

The authors declare no conflict of interest.

Data Availability Statement

The data that support the findings of this study are available in the supplementary material of this article.

Keywords

flowerlike nanoplates, initiated chemical vapor deposition, oil clean-up, photocatalytic layer, selective oil adsorption

Received: October 30, 2021

Revised: January 25, 2022

Published online: March 2, 2022

- [1] M. I. Ramirez, A. P. Arevalo, S. Sotomayor, N. Bailon-Moscoso, *Environ. Pollut.* **2017**, 231, 415.
- [2] A. B. Nordvik, J. L. Simmons, K. R. Biting, A. Lewis, T. Strøm-Kristiansen, *Spill Sci. Technol. Bull.* **1996**, 3, 107.
- [3] Z. Chu, Y. Feng, S. Seeger, *Angew. Chem., Int. Ed.* **2015**, 54, 2328.
- [4] G. Deschamps, H. Caruel, M. E. Borredon, C. Bonnin, C. Vignoles, *Environ. Sci. Technol.* **2003**, 37, 1013.
- [5] R. J. Archer, B. Becher-Nienhaus, G. J. Dunderdale, A. Hozumi, *Adv. Funct. Mater.* **2020**, 30, 1907772.
- [6] L. Yan, X. Yang, Y. Zhao, Y. Wu, R. Motilhalets Moutloali, B. B. Mamba, P. Sorokin, L. Shao, *Sep. Purif. Technol.* **2022**, 285, 120383.
- [7] J. Ge, H. Y. Zhao, H. W. Zhu, J. Huang, L. A. Shi, S. H. Yu, *Adv. Mater.* **2016**, 28, 10459.
- [8] X. Feng, L. Jiang, *Adv. Mater.* **2006**, 18, 3063.
- [9] H.-M. Choi, J. P. Moreau, *Microsc. Res. Tech.* **1993**, 25, 447.
- [10] M. Paven, L. Mammen, D. Vollmer, *RSC Smart Mater.* **2016**, 20, 209.
- [11] B. Tansel, M. Lee, *J. Environ. Manage.* **2019**, 247, 363.
- [12] J. Wu, F. Xu, S. Li, P. Ma, X. Zhang, Q. Liu, R. Fu, D. Wu, *Adv. Mater.* **2019**, 31, 1802922.
- [13] M. Pumera, *Chem. Commun.* **2011**, 47, 5671.
- [14] S. Veziroglu, M. Z. Ghor, A. Obermann, K. Röder, O. Polonskyi, T. Strunskus, F. Faupel, O. C. Aktas, *Phys. Status Solidi* **2019**, 216, 1800898.
- [15] G. P. Lee, Y. Shi, E. Lavoie, T. Daeneke, P. Reineck, U. B. Cappel, D. M. Huang, U. Bach, *ACS Nano* **2013**, 7, 5911.
- [16] H. Yu, Q. Zhang, H. Liu, M. Dahl, J. B. Joo, N. Li, L. Wang, Y. Yin, *ACS Nano* **2014**, 8, 10252.
- [17] R. W. Berriman, R. H. Herz, *Nature* **1957**, 180, 293.
- [18] S. Tougaard, *Microsc. Microanal.* **2005**, 11, 2005.
- [19] G. Aresta, J. Palmans, M. C. M. van de Sanden, M. Creatore, *J. Vac. Sci. Technol., A* **2012**, 30, 041503.
- [20] S. Schröder, O. Polonskyi, T. Strunskus, F. Faupel, *Mater. Today* **2020**, 37, 35.
- [21] T. Watanabe, A. Nakajima, R. Wang, M. Minabe, S. Koizumi, A. Fujishima, K. Hashimoto, *Thin Solid Films* **1999**, 351, 260.
- [22] O. Carp, C. L. Huisman, A. Reller, *Prog. Solid State Chem.* **2004**, 32, 33.
- [23] J. Shondo, S. Veziroglu, D. Stefan, Y. K. Mishra, T. Strunskus, F. Faupel, O. C. Aktas, *Appl. Surf. Sci.* **2021**, 537, 147795.
- [24] D. Soto, A. Ugur, T. A. Farnham, K. K. Gleason, K. K. Varanasi, *Adv. Funct. Mater.* **2018**, 28, 1707355.
- [25] M. A. Gondal, M. S. Sadullah, M. A. Dastageer, G. H. McKinley, D. Panchanathan, K. K. Varanasi, *ACS Appl. Mater. Interfaces* **2014**, 6, 13422.
- [26] M. J. Kreder, J. Alvarenga, P. Kim, J. Aizenberg, *Nat. Rev. Mater.* **2016**, 1, 15003.
- [27] O. C. Aktas, S. Schröder, S. Veziroglu, M. Z. Ghor, A. Haidar, O. Polonskyi, T. Strunskus, K. Gleason, F. Faupel, *Adv. Mater. Interfaces* **2019**, 6, 1801967.
- [28] N. Atthi, W. Sripumkhai, P. Pattamang, O. Thongsook, R. Meananetra, P. Saengdee, N. Ranron, K. Pankong, W. Uahchinkul, S. Radomyos, A. Srihapat, J. Supadech, N. Klunngien, W. Jeamsaksiri, *Jpn. J. Appl. Phys.* **2021**, 60, SCC01.
- [29] D. S. Kilin, O. V. Prezhd, Y. Xia, *Chem. Phys. Lett.* **2008**, 458, 113.
- [30] T. Zubkov, D. Stahl, T. L. Thompson, D. Panayotov, O. Diwald, J. T. Yates, T. Zubkov, D. Stahl, T. L. Thompson, D. Panayotov, O. Diwald, J. T. Yates, *J. Phys. Chem. B* **2005**, 109, 15454.
- [31] Q. Ruan, T. Miao, H. Wang, J. Tang, *J. Am. Chem. Soc.* **2020**, 142, 2795.
- [32] H. Moon, H. Seong, W. C. Shin, W. T. Park, M. Kim, S. Lee, J. H. Bong, Y. Y. Noh, B. J. Cho, S. Yoo, S. G. Im, *Nat. Mater.* **2015**, 14, 628.
- [33] T. Kamegawa, K. Irikawa, H. Yamashita, *Sci. Rep.* **2017**, 7, 13628.
- [34] A. O. Ibadon, G. M. Greenway, Y. Yue, *Catal. Commun.* **2008**, 9, 153.
- [35] K. P. O. Mahesh, D.-H. Kuo, B.-R. Huang, M. Ujihara, T. Imae, *Appl. Catal. A Gen.* **2014**, 475, 235.
- [36] S. Cho, W. Choi, *J. Photochem. Photobiol., A* **2001**, 143, 221.
- [37] V. Senthikumar, M. Jayachandran, C. Sanjeeviraja, *Thin Solid Films* **2010**, 519, 991.
- [38] H. Fakhouri, J. Pulpytel, W. Smith, A. Zolfaghari, H. R. Mortaheb, F. Meshkini, R. Jafari, E. Sutter, F. Arefi-Khonsari, *Appl. Catal., B* **2014**, 144, 12.
- [39] J. Tauc, R. Grigorovici, A. Vancu, *Phys. Status Solidi* **1966**, 15, 627.
- [40] C. Adomniti, S. Tascu, D. Luca, M. Dobromir, M. Girtan, D. Mardare, *Bull. Mater. Sci.* **2015**, 38, 1259.
- [41] S. Pan, A. K. Kota, J. M. Mabry, A. Tuteja, *J. Am. Chem. Soc.* **2013**, 135, 578.
- [42] G. B. D. Briggs, *J. Chem. Educ.* **1993**, 70, A25.
- [43] S. Veziroglu, A.-L. Obermann, M. Ullrich, M. Hussain, M. Kamp, L. Kienle, T. Leifner, H.-G. Rubahn, O. Polonskyi, T. Strunskus, J. Fiutowski, M. Es-Souni, J. Adam, F. Faupel, O. C. Aktas, *ACS Appl. Mater. Interfaces* **2020**, 12, 14983.
- [44] M. Z. Ghor, S. Veziroglu, B. Henkel, A. Vahl, O. Polonskyi, T. Strunskus, F. Faupel, O. C. Aktas, *Sol. Energy Mater. Sol. Cells* **2018**, 178, 170.
- [45] A. Vahl, S. Veziroglu, B. Henkel, T. Strunskus, O. Polonskyi, O. C. Aktas, F. Faupel, *Materials* **2019**, 12, 2840.
- [46] S. Schröder, T. Strunskus, S. Rehders, K. K. Gleason, F. Faupel, *Sci. Rep.* **2019**, 9, 2237.
- [47] S. Schröder, A. M. Hinz, T. Strunskus, F. Faupel, *J. Phys. Chem. A* **2021**, 125, 1661.
- [48] R. Tadmor, *Langmuir* **2004**, 20, 7659.